Functional recovery with recombinant human IGF1 treatment in a mouse model of Rett Syndrome

Jorge Castro[a,1], Rodrigo I. Garcia[a,1], Showming Kwok[a], Abhishek Banerjee[a], Jeremy Petravicz[a], Jonathan Woodson[a], Nikolaos Mellios[a], Daniela Tropea[b], and Mriganka Sur[a,2]

[a]Department of Brain and Cognitive Sciences, Picower Institute for Learning and Memory, Massachusetts Institute of Technology, Cambridge, MA 02139; and [b]Neuropsychiatric Genetics Department, Trinity Center for Health Sciences, St. James Hospital, Dublin D8, Ireland

Edited* by Michael Merzenich, Brain Plasticity Institute, San Francisco, CA, and approved May 28, 2014 (received for review June 20, 2013)

Rett Syndrome is a neurodevelopmental disorder that arises from mutations in the X-linked gene methyl-CpG binding protein 2 (*MeCP2*). MeCP2 has a large number of targets and a wide range of functions, suggesting the hypothesis that functional signaling mechanisms upstream of synaptic and circuit maturation may contribute to our understanding of the disorder and provide insight into potential treatment. Here, we show that insulin-like growth factor-1 (IGF1) levels are reduced in young male *Mecp2*-null (*Mecp2*$^{-/y}$) mice, and systemic treatment with recombinant human IGF1 (rhIGF1) improves lifespan, locomotor activity, heart rate, respiration patterns, and social and anxiety behavior. Furthermore, *Mecp2*-null mice treated with rhIGF1 show increased synaptic and activated signaling pathway proteins, enhanced cortical excitatory synaptic transmission, and restored dendritic spine densities. IGF1 levels are also reduced in older, fully symptomatic heterozygous (*Mecp2*$^{-/+}$) female mice, and short-term treatment with rhIGF1 in these animals improves respiratory patterns, reduces anxiety levels, and increases exploratory behavior. In addition, rhIGF1 treatment normalizes abnormally prolonged plasticity in visual cortex circuits of adult *Mecp2*$^{-/+}$ female mice. Our results provide characterization of the phenotypic development of Rett Syndrome in a mouse model at the molecular, circuit, and organismal levels and demonstrate a mechanism-based therapeutic role for rhIGF1 in treating Rett Syndrome.

molecular therapeutic | respiration | synaptic function | male mice | female mice

Rett Syndrome (RTT) is a devastating, rare neurodevelopmental disorder that primarily afflicts girls. Over 90% of individuals with RTT have sporadic mutations in the X-linked gene coding for methyl-CpG binding protein 2 (MeCP2). Affected girls are initially asymptomatic, but later develop a wide range of symptoms. Mouse models of RTT with deletion of *Mecp2* recapitulate many of the key physiological, autonomic, motor, and cognitive aspects of the disorder (1, 2).

MeCP2 binds widely across the genome and has complex roles that encompass activating or inhibiting gene transcription, repressing methylation, regulating chromatin remodeling, and altering noncoding RNAs (3). This wide range of functions has led to the proposal that a focus on functional signaling pathways is needed to drive an understanding of RTT and its possible therapeutics (1, 2, 4). Several lines of evidence indicate an arrested brain maturation phenotype in RTT, suggesting that loss of functional MeCP2 leads to immature synapses and circuits in the brain (5). Importantly, mouse models have suggested reversibility of specific symptoms once MeCP2 function is restored (6, 7). One well-documented target of MeCP2 is brain-derived neurotrophic factor (BDNF), which is known to be critical for neuronal and synaptic maturation and is down-regulated in *Mecp2* mutant mice and RTT patients (8, 9). BDNF exerts influence on neurons and synapses mainly via the phosphoinositide 3-kinase (PI3K)/Akt pathway and the extracellular signal-regulated kinase (ERK) pathways (10), which are also down-regulated in several brain regions of *Mecp2* mutant mice (11, 12). Overexpression of BDNF has been shown to reverse some symptoms of the mutant phenotype, pointing to the importance of BDNF and its downstream signaling pathways as therapeutic targets for RTT (8). Unfortunately, little BDNF is able to traverse the blood brain barrier (BBB), making it unsuitable as a therapeutic agent (13).

Another major activator of these signaling pathways is insulin-like growth factor-1 (IGF1), which is primarily expressed in the liver and acts in an endocrine fashion throughout the body, crossing the BBB in a neuronal activity-dependent manner (14); IGF1 is also produced in the brain, especially during early stages of development (15, 16). A previous study showed that administering the tripeptide fragment Glutamate–Proline–Glycine (GPE) or (1–3)IGF1, the first 3 (of 70) amino acids of IGF1, to *Mecp2* KO mice was effective in correcting several symptoms and restoring key synaptic molecules (5). We have now examined, for the first time to our knowledge, the effectiveness of full-length IGF1 in both *Mecp2*-null male (*Mecp2*$^{-/y}$) and older symptomatic heterozygous female (*Mecp2*$^{-/+}$) mice (17). We show that administering full-length, recombinant human IGF1 (rhIGF1, Mecasermin DB01277) to the mutant mice increases IGF1 concentration in serum to near-normal levels and ameliorates a wide range of phenotypes, including organismal and behavioral function, synaptic and circuit plasticity, neuronal structure, and molecular signaling pathways. Together with recent and ongoing clinical trials demonstrating the safety and efficacy of rhIGF1 in treating RTT (18, 19), and multiple studies documenting the effectiveness of IGF1 in restoring structural, functional, and molecular phenotypes in human induced pluripotent stem cell (iPSC)-derived RTT neurons and glia (20–22), our results provide strong mechanistic

Significance

Rett Syndrome is a devastating neurodevelopmental disorder that arises from mutations in the methyl-CpG binding protein 2 (*MeCP2*) gene and has no presently available treatment. We show that levels of insulin-like growth factor-1 (IGF1) are reduced in male and female *Mecp2* mutant mice. Treating male knockout mice with recombinant human IGF1 (rhIGF1) improves a range of physiological symptoms and behaviors, increases excitatory transmission and synapse density in cortical neurons, and up-regulates molecular signals underlying these deficits. Treating symptomatic female heterozygous mice also improves a range of physiological and behavioral symptoms and normalizes maturation of cortical circuits. These findings demonstrate that rhIGF1 corrects functional, structural, and molecular mechanisms downstream of MeCP2 and may be an effective therapeutic for Rett Syndrome.

Author contributions: J.C., R.I.G., S.K., and M.S. designed research; J.C., R.I.G., S.K., A.B., J.P., J.W., N.M., and D.T. performed research; J.C., R.I.G., S.K., A.B., J.P., J.W., N.M., and D.T. analyzed data; and J.C., R.I.G., S.K., and M.S. wrote the paper.

The authors declare no conflict of interest.

*This Direct Submission article had a prearranged editor.

[1]J.C. and R.I.G. contributed equally to this work.

[2]To whom correspondence should be addressed. E-mail: msur@mit.edu.

This article contains supporting information online at www.pnas.org/lookup/suppl/doi:10.1073/pnas.1311685111/-/DCSupplemental.

and preclinical support for the therapeutic role of rhIGF1 in RTT.

Results

The Physiological Condition and Social Behavior of *Mecp2*-Null Animals Are Affected by Decreased Levels of Endogenous IGF1 and Are Improved with rhIGF1 Treatment. We first examined whether endogenous IGF1 levels were decreased in $Mecp2^{-/y}$ mice (on a C57BL/6J background) and found that there was indeed significantly less serum IGF1 in postnatal day 28 (P28) $Mecp2^{-/y}$ mice compared with age-matched controls (Fig. 1*A*). The difference was less pronounced but still significant at P56, consistent with the fact that levels of endogenous IGF1 reach peak concentration during puberty. To test the effects of an increase in systemic IGF1 by administration of rhIGF1, a battery of tests aimed to evaluate the health status, locomotion, and vital signs were carried out on a regular schedule (Fig. S1*A*). $Mecp2^{-/y}$ mice that were injected intraperitoneally (i.p.) starting at P14 with a daily dose (0.25 mg/kg) of rhIGF1 had an increased lifespan compared with vehicle-treated $Mecp2^{-/y}$ mice (Fig. 1*B* and Fig. S1*B*). This improvement in life expectancy was accompanied by an increase in weight when measured at P56—a time point when mutant animals are fully symptomatic (Fig. 1*C*). RTT patients show periods of both apnea and bradycardia, which increases the likelihood of sudden death in some patients. Pulse oximeter monitoring allows for the simultaneous investigations of heart and breath rates from nonanesthetized animals, and $Mecp2^{-/y}$ mice had lower breathing and heart rates as early as P28. Treatment with rhIGF1 improved both metrics after 6 wk of daily treatment (Fig. 1 *D* and *E*).

The shortened lifespan of the $Mecp2^{-/y}$ mice is preceded by a sharp decline in locomotor activity in the form of lethargy and hypokinesia (23). $Mecp2^{-/y}$ mice showed an age-dependent decline in their nocturnal movements compared with their WT littermates; by P56, the untreated mutant mice suffered a pronounced decrease in locomotion, whereas age-matched treated animals showed significantly greater locomotor activity (Fig. 1*F*).

To evaluate social behavior, we selected tests such as the three-chamber test and elevated plus maze that require relatively low motor activity (Fig. S1*C*). In the three-chamber test (a social preference task), both the WT and $Mecp2^{-/y}$ mice spent more time in the chamber containing a stranger mouse, indicating similar tendencies for social contact. However, when the same stranger animal was presented 30 min after the first exposure, untreated $Mecp2^{-/y}$ mice did not show the usual habituation and decrease in interest that both age-matched WT groups and treated mutant mice displayed (Fig. 1*G*). This behavior was similarly evident at P56 (Fig. S1*D*). No positional bias was observed (Fig. S1*E*).

In the elevated plus maze, a test used to measure the level of anxiety, we found that untreated $Mecp2^{-/y}$ mice spent more time in the open arms compared with their WT and treated littermates (Fig. 1*H*). Conversely, the untreated $Mecp2^{-/y}$ mice did not show a preference for the closed arms (Fig. S1*F*) as was seen in WT and mutant treated animals. This behavior was not due to abnormal exploratory activity, as the number of crosses to the open arms was similar across groups (Fig. S1*G*).

rhIGF1 Treatment Curtails Abnormally Prolonged Visual Cortical Plasticity. RTT symptoms may arise from prolonged immaturity of synapses and circuits in the brain (1). By using optical imaging of intrinsic signals from layers 2/3 of primary visual cortex (V1) in vivo, we measured the responses driven by eye-specific stimulation in normally developing animals or after monocular deprivation (MD) of one eye for 4 consecutive days. The ratio between the cortical responses driven by the deprived (contralateral) eye and the nondeprived (ipsilateral) eye, known as the Ocular Dominance Index (ODI), provides a robust measure of the ability of visual cortex circuits to reorganize in response to changes in eye-specific drive (Fig. 2*A*). Such plasticity is prominent during a critical period of development, when synapses and circuits are still maturing—peaking around P28 in WT mice and declining afterward, due to further cortical maturation (24). We examined cortical plasticity at P28 and P60 (Fig. 2*B*); because $Mecp2^{-/y}$ mice develop severe symptoms by P60 and often cannot tolerate experiments involving anesthesia, we used *Mecp2* heterozygous female ($Mecp2^{-/+}$) mice, which show less severe symptoms at these ages. Ocular dominance plasticity at P28 in $Mecp2^{-/+}$ mice was comparable to that in WT mice (Fig. 2 *C* and *D*): MD reduced the response amplitude from the deprived contralateral eye and shifted the ODI toward the nondeprived ipsilateral eye, indicating normal critical period plasticity. By P60, WT mice showed stable visual cortex circuits with no change in eye-specific responses or a shift in the ODI after MD. In contrast, age-matched $Mecp2^{-/+}$

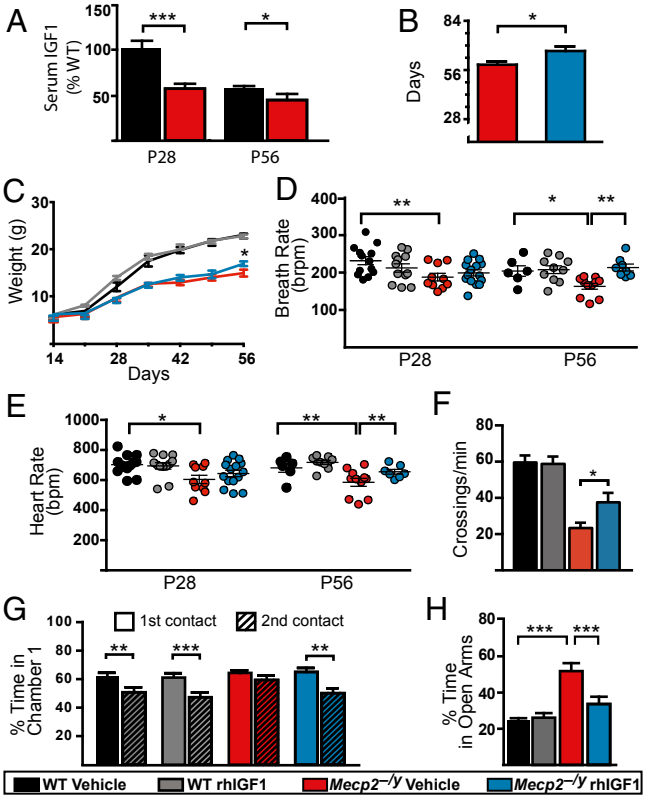

Fig. 1. rhIGF1 promotes survival, improves physiological condition, and restores normal levels of social and anxiety-related behavior of $Mecp2^{-/y}$ mice. (*A*) Serum levels of endogenous IGF1 measured in P28 and P56 mice relative to WT P28 controls [statistical comparisons used unpaired *t* test for equal variances; WT (P28 and P56), $n = 12$ and 10; $Mecp2^{-/y}$ (P28 and P56), $n = 10$ and 9]. (*B*) Mean survival age of $Mecp2^{-/y}$ animals treated with vehicle or rhIGF1 (unpaired *t* test; $Mecp2^{-/y}$ vehicle, $n = 27$; rhIGF1, $n = 29$). (*C*) Weight variation from P14 (starting day of injection) to P56. Comparisons between KO vehicle and treated were done week by week with an unpaired *t* test for equal variances (WT vehicle, $n = 26$; rhIGF1, $n = 22$; $Mecp2^{-/y}$ vehicle, $n = 27$; rhIGF1, $n = 29$). (*D* and *E*) Scatterplot of average breathing (*D*) and cardiac (*E*) rates. Each dot represents a single animal; lines indicate population average (ANOVA with Newman–Keuls post hoc analysis for multiple comparison). (*F*) Nocturnal locomotor activity expressed as average number of beam crossings per minute (ANOVA with Newman–Keuls post hoc analysis for multiple comparisons performed at each separate time point; WT vehicle, $n = 25$; rhIGF1, $n = 28$; $Mecp2^{-/y}$ vehicle, $n = 21$; rhIGF1, $n = 26$). (*G*) Three-chamber test measurements showing the percentage of time the animals spent socializing with a stranger mouse during the first contact (solid bars) and 30 min after the first contact (hatched bars) at P28–35 (paired *t* test). (*H*) Percentage of time spent in the open arms of a plus maze as measurement of anxiety-related behavior at P28–35 (ANOVA with Newman–Keuls post hoc analysis for multiple comparisons; WT vehicle, $n = 18$; rhIGF1, $n = 16$; $Mecp2^{-/y}$ vehicle, $n = 21$; rhIGF1, $n = 23$). Error bars represent SEM. $^*P < 0.05$; $^{**}P < 0.01$; $^{***}P < 0.001$. See also Fig. S1.

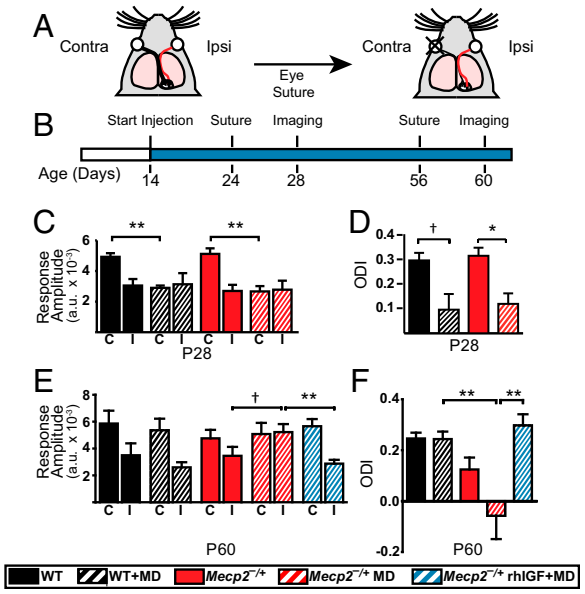

Fig. 2. Curtailment of abnormal visual cortical plasticity by rhIGF1 treatment. (*A*) Schematic showing MD paradigm. Black and red lines, respectively, depict the contralateral and ipsilateral projections that connect the deprived (contralateral) and nondeprived (ipsilateral) eye to V1. (*B*) Experimental timeline for treatment, eyelid suture, and optical imaging. (*C*) Average response amplitudes measured in V1 from the deprived contralateral (C) and nondeprived ipsilateral (I) eye in P28 female mice (Mann–Whitney test; WT and WT+MD, $n = 3$ each; *Mecp2*$^{-/+}$, $n = 4$; *Mecp2*$^{-/+}$+MD, $n = 4$ each). (*D*) Average ODI values in P28 females (Mann–Whitney test). (*E*) Response amplitudes observed in P60 females (Mann–Whitney test; $n = 5$ for each group). (*F*) ODI representation for P60 females for each condition (ANOVA with Newman–Keuls post hoc analysis for multiple comparisons). Error bars represent SEM. $^{\dagger}P < 0.10$; $*P < 0.05$; $**P < 0.01$.

mice still showed a shift in ODI, largely due to an abnormal increase in responses from the nondeprived eye (Fig. 2*E*). This effect was abolished following treatment with rhIGF1, consistent with rhIGF1 curtailing this late-persisting ocular dominance plasticity (Fig. 2*F*).

rhIGF1 Improves Excitatory Transmission and Spine Density in Visual Cortex Neurons While Activating Signaling Pathways and Downstream Synaptic Proteins. To assess the effect of *Mecp2* deletion and rhIGF1 treatment on excitatory synaptic transmission in cortical neurons, we conducted whole-cell voltage clamp recordings of miniature excitatory postsynaptic currents (mEPSCs) from layer 2/3 pyramidal neurons in the visual cortex of *Mecp2*$^{-/y}$ mice. Treatment of *Mecp2*$^{-/y}$ mice with rhIGF1 induced a significant increase in mEPSC amplitudes and shifted the distribution to a level comparable to that in WT mice (Fig. 3 *A* and *B* and Fig. S2*A*). Application of 10 μM 6-cyano-7-nitroquinoxaline-2,3-dione significantly blocked the occurrence of mEPSCs, indicating that the recorded events were AMPA receptor-mediated (Fig. S2*B*). The frequency of mEPSCs examined by the interevent interval distributions was unchanged between *Mecp2*$^{-/y}$ and WT control mice (Fig. S2*C*), indicating that the changes in amplitude were likely to be postsynaptic in nature.

We hypothesized that the observed modifications of circuit-level plasticity and changes in synaptic strength could be explained by alterations of synaptic connectivity as well as the molecular underpinnings of these processes. We measured the spine density of layer 2/3 visual cortex basal dendrites in *Mecp2*$^{-/y}$ mice as a structural correlate of connectivity and functional plasticity. Spine densities showed a significant decrease in the mutant mice and recovery with rhIGF1 treatment (Fig. 3*C*). Cortical synaptic PSD95, a postsynaptic protein necessary for glutamate receptor organization and functional responses to plasticity (25, 26), can be regulated by the activation of upstream signaling pathways, in particular the key effectors Akt and ERK1/2 (27) (Fig. 3*D*). Quantification of synaptic PSD95 levels measured at P28 from *Mecp2*$^{-/y}$ mice, after 2 wk of rhIGF1 treatment, showed a significant increase in treated mice compared with vehicle-treated KO littermates (Fig. 3*E*, *Left*). Consistent with these findings, the ratio of phosphorylated to total Akt and ERK1/2 in cortical whole-cell homogenates showed an increase in rhIGF1-treated *Mecp2*$^{-/y}$ mice compared with the vehicle-treated KO animals (Fig. 3*E*, *Center* and *Right*). Thus, rhIGF1 leads to an increase in neuronal signaling pathways that underlie structural and functional maturation of synapses.

rhIGF1 Treatment Increases the Availability of Total IGF1. Because serum IGF1 levels are reduced in *Mecp2*$^{-/y}$ mice (Fig. 1*A*), we examined whether and how exogenous application of rhIGF1 affected the concentration of IGF1. Previous studies have established a correlation between serum levels of IGF1 and those found in the brain (28); therefore, the levels of total IGF1 in serum provide an initial measurement of the potential availability in the brain. Serum levels of rhIGF1 and endogenous murine IGF1 were measured at P28 and P56 using type-specific sandwich ELISA for each species. Samples were taken 2 and 24 h postinjection, which would allow for the uptake of rhIGF1 into the bloodstream as well as provide an indication of drug clearance time (Fig. S3*A*). In P28 *Mecp2*$^{-/y}$ mice, following 2 wk of treatment, we observed a significant increase in serum levels of rhIGF1

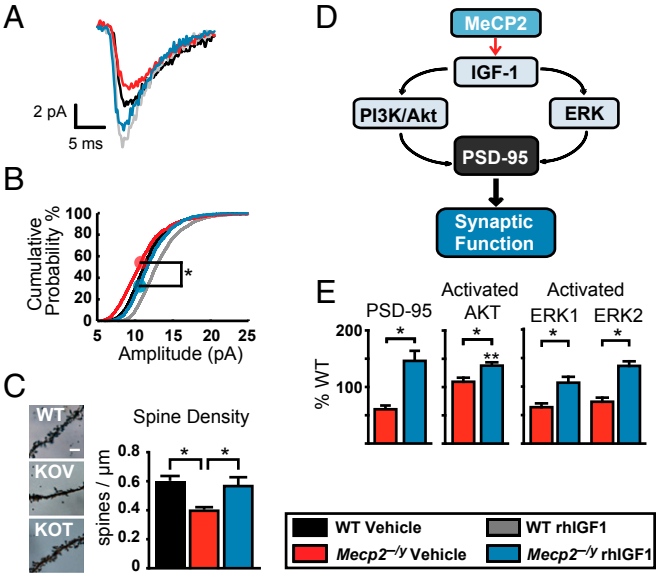

Fig. 3. Effects of rhIGF1 on excitatory synaptic transmission, spine density, and signaling pathways. (*A*) Averaged mEPSCs from V1 layer 2/3 cells comparing peak amplitudes (events: WT vehicle, $n = 270$; WT rhIGF1, $n = 816$; KO vehicle, $n = 354$; KO rhIGF1, $n = 268$). (*B*) Distribution of mEPSC amplitude across all cells. rhIGF1 treatment significantly shifted the population distribution toward higher peak amplitudes (Kolmogorov–Smirnov test between vehicle and treated *Mecp2*$^{-/y}$ with pooled data from five to eight cells from three to four animals in each group). (*C*) Representative micrographs of basal dendrites in supragranular pyramidal neurons at P42 stained with Golgi and their synaptic spine density measurements (one-way ANOVA with Newman–Keuls post hoc analysis for multiple comparisons). (Scale bar, 5 μm.) (*D*) Schematic of proposed signaling pathways downstream of MeCP2-mediated IGF1 activation. (*E*) Quantification of PSD95 (*Left*) Western blots in synaptoneurosomes as a percentage of WT littermate control levels and the ratios between phosphorylated and total Akt (*Center*) and ERK1/2 (*Right*) in whole-cell homogenates. Ratios are based on Western blot protein measurements at P28 (comparisons used a one-way ANOVA with Newman–Keuls post hoc analysis for multiple comparisons including WT controls). $*P < 0.05$; $**P < 0.01$. Error bars represent SEM. See also Fig. S2.

NEUROSCIENCE

2 h postinjection (Fig. 4*A*). However, this increase was lower in treated *Mecp2*$^{-/y}$ animals compared with the WT treated animals. A second set of measurements taken at P56, after 6 wk of daily treatment, showed a similar pattern of rhIGF1 increase, yet with lower levels in the *Mecp2*$^{-/y}$ mice; furthermore, the P56 levels were lower than at P28 in the mutant mice. Taken together, these results point to a combined effect of MeCP2 function and treatment length as variables influencing availability of the administered rhIGF1. To further explore these results, we tested P56 animals that received only a 1-wk treatment and found that rhIGF1 availability in both WT and mutant mice was now comparable to their respective levels at P28 (Fig. 4*A*), implying that the availability of rhIGF1 decreased after prolonged daily injections. Thus, a strategy of intermittent treatment may be effective in elevating serum IGF1. Total levels of IGF1, calculated as a sum of injected rhIGF1 plus endogenous IGF1, were increased in the treated animals across the entire treatment period (Fig. 4*B*). Of note, treated groups, compared with the corresponding genetically matched untreated groups, did not show a significant decrease in endogenous IGF1 even after 6 wk of treatment (Fig. 4*B*, filled boxes). Thus, rhIGF1 treatment contributes significantly to increasing total serum IGF1 and does not reduce endogenous IGF1 production.

We also examined whether a higher concentration of rhIGF1 might be more effective in increasing serum IGF1. Administering a 10-fold higher dose of rhIGF1 (2.5 mg/kg, 10×) from P14 to P28 led to higher rhIGF1 serum levels compared with the regular dose (0.25 mg/kg, 1×) littermates treated for a similar duration. Nevertheless, this high-dosage treatment did not lead to an increase in total serum IGF1 in the *Mecp2*$^{-/y}$ mice due to a concomitant decrease in endogenously synthesized IGF1 (Fig. S3*B*). Consistent with this finding, autonomic function was similar in the high-dose compared with the low-dose animals (Fig. S3*C*).

Short-Term Treatment with rhIGF1 Improves Breathing Patterns and Behavioral Deficits in Symptomatic *Mecp2*$^{-/+}$ Females. RTT primarily affects females and the severity of the disease can vary greatly due to the specific mutation and the mosaic expression of MeCP2 caused by X-chromosome inactivation (29–31). To further examine the therapeutic potential of rhIGF1, we sought to test its efficacy in female heterozygous (*Mecp2*$^{-/+}$) mice that present a more heterogeneous disease severity as well as a later time of onset (23, 32, 33). We therefore chose to use older, symptomatic females of various ages (>6 mo) and a 10× treatment dose to maximize the potential effects during a 3-wk daily treatment regimen. Despite the inherent variability, we were able to test physiological and behavioral parameters pre- and posttreatment on the same animals, allowing for more robust statistical analysis. We first investigated the detailed breathing patterns exhibited by the *Mecp2*$^{-/+}$ mice by using a whole-body plethysmograph. Previous studies in human patients and mouse models have shown abnormal postinspiratory times (34–36). We found irregular patterns with reduced inspiratory and prolonged expiratory times, along with reduced peak expiratory amplitudes, that were strikingly rescued with rhIGF1 treatment (Fig. 5 *A* and *B* and Fig. S4 *C*–*E*). Apneas and breath holds are a hallmark phenotype of RTT, and we observed a high number of breath holds that was subsequently reduced posttreatment (Fig. 5*C*).

Mecp2$^{-/+}$ mice have been shown to exhibit cognitive-associated deficits in tests for spatial recognition and anxiety (23). We found that *Mecp2*$^{-/+}$ female mice had improved performance on recognition of spatial rearrangement following 3 wk of treatment (Fig. 5*D*). Additionally, as with the anxiety-related measurements in younger KO males, these females spent more time in the open arms of the elevated plus maze before treatment and had a significant posttreatment reduction (Fig. 5*E*). In contrast to these improvements in cognitive functions and unlike the effects seen in young males, the short period of rhIGF1 treatment did not improve social recognition performance in the three-chamber test (Fig. S4*F*) or hypoactivity (Fig. S4*G*). Finally, older symptomatic females also showed a relative reduction in serum IGF1 levels compared with WT controls, and levels of total available serum IGF1 posttreatment were elevated to be similar to WT controls (Fig. 5*F*).

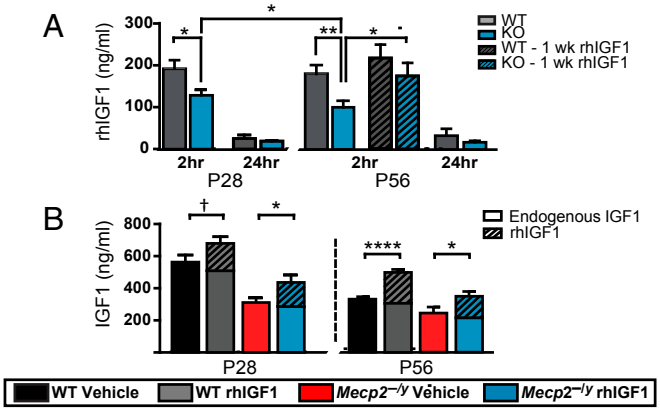

Fig. 4. Measurement of rhIGF1 levels and IGF1 availability. (*A*) Levels of rhIGF1 in serum collected 2 and 24 h after i.p. injection of rhIGF1 (unpaired *t* test; *n* animals at P28, 2 and 24 h: WT, 14 and 7; *Mecp2*$^{-/y}$, 22 and 7; *n* animals at P56, 2 and 24 h: WT, 18 and 5; *Mecp2*$^{-/y}$, 18 and 6). See Fig. S3*A*. Hatched bars show measurements in P56 mice after 1 wk of treatment ($n = 4$ each). (*B*) Total IGF1 concentration in blood serum collected after 2 h calculated by addition of endogenous IGF1 (filled boxes) and rhIGF1 (hatched boxes) levels for each animal. Statistics were calculated with the summed values [one-way ANOVA with Newman–Keuls post hoc analysis for multiple comparisons of treatment effects, separate analysis for each age; WT (P28 and P56), $n = 12$ and 10; WT+rhIGF1 (P28 and P56), $n = 10$ and 15; *Mecp2*$^{-/y}$ (P28 and P56), $n = 10$ and 9; *Mecp2*$^{-/y}$+rhIGF1 (P28 and P56), $n = 11$ and 12]. Error bars represent SEM. $^{\dagger}P < 0.1$; $^{*}P < 0.05$; $^{**}P < 0.01$; $^{****}P < 0.0001$. See also Fig. S3.

Discussion

We have shown that IGF1 levels are reduced in an established mouse model of RTT (*Mecp2*$^{tm1.1Bird}$ on a C57BL/6J background) and that treatment with full-length rhIGF1 increases serum IGF1 concentration and ameliorates a wide range of phenotypes. RTT patients show similar lower levels of IGF1 in cerebral spinal fluid (19). A treatment regimen with the same dose of rhIGF1 increases IGF1 levels, with a safety profile that yields few negative side effects following administration for 4 wk or longer, and an efficacy profile that ameliorates specific symptoms including cardiorespiratory function and anxiety (18, 19). IGF1 levels are regulated by MeCP2 via the let-7 family of micro RNAs (28). Thus, any treatment increasing the level of IGF1 would not only augment the activation of signaling pathways shared with BDNF, a well-known target of MeCP2 that is significantly decreased when *Mecp2* is mutated, but also reverse the deficit of IGF1. Our findings stand in contrast to a recent study that examined the effects of full-length IGF1 modified with the addition of polyethylene glycol (PEG–IGF1) treatment in *Mecp2* KO mice (*Mecp2*$^{tm1.1Bird}$) on a mixed background (B6129S6F1) and showed variable effects, in particular on body weight, metabolism, and lifespan (37). However, it is well established that the same genetic manipulation can exhibit profoundly different phenotypes when present on different genetic backgrounds (38), and the 129 strains exhibit anomalous glucose and insulin metabolism (39, 40). Indeed, *Mecp2* KO mice (*Mecp2*$^{tm1.1Bird}$) when mixed with 129 strains show an increase in body weight, whereas the same KO animals maintained on a C57BL/6 background have lower body weight (41–43). This phenotype would be further exacerbated by the slow pharmacokinetics of PEG–IGF1: Serum IGF1 concentration in treated animals was not consistently measured in this study, but would be expected to be abnormally high, particularly at high PEG–IGF1 doses that may lead to buildup effects (44), thus contributing to the negative effects. In the

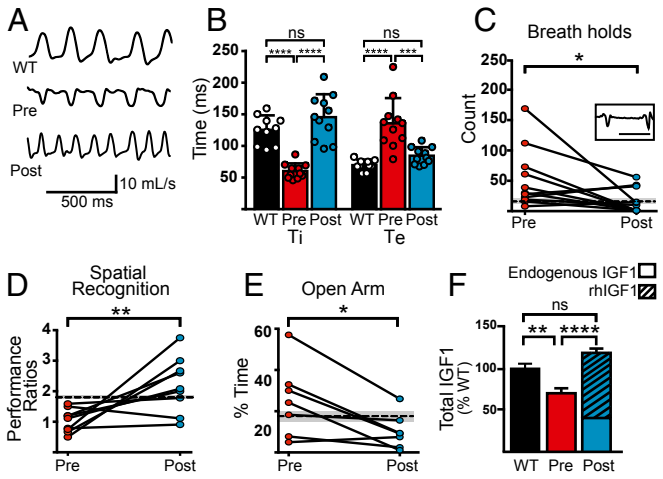

Fig. 5. Effects of rhIGF1 on *Mecp2*$^{-/+}$ breathing patterns, anxiety, and spatial recognition. (*A*) Representative breathing pattern traces of WT (*Top*) and *Mecp2*$^{-/+}$ females before (*Middle*) and after (*Bottom*) treatment. Downward indicates inspiration (Fig. S4*C*). (*B*) Average inspiratory (Ti) and expiratory (Te) times were abnormal in *Mecp2*$^{-/+}$ females, and treatment restored these to WT levels (paired *t* test for post/pre comparison and ordinary one-way ANOVA with Tukey's post hoc analysis for multiple comparisons). Dots represent individual animals. (*C*) Total number of breath holds observed during 12-min recording sessions pre- and posttreatment (paired *t* test). Inset shows representative breath hold trace from a pretreatment female. (Scale bar, 500 ms.) (*D*) Performance ratio of time spent with displaced versus nondisplaced objects (see *Materials and Methods* for details of assay) pre- and posttreatment (paired *t* test). (*E*) Percent time spent in the open arms of elevated plus maze pre- and posttreatment (paired *t* test). (*F*) Relative serum levels of total IGF1 (murine and rhIGF1) measured pre- and posttreatment (one-way ANOVA with Tukey's post hoc analysis for multiple comparison). Error bars represent S.E.M. $*P < 0.05$; $**P < 0.01$; $****P < 0.0001$. In *C*–*E*, dashed line and gray shading represent mean and SEM of WT mice, respectively. See also Fig. S4.

present study, females receiving a higher, short-term dose did not show any significant alterations in weight (Fig. S4 *A* and *B*).

Systemic treatment with rhIGF1 improves organismal function, specific behaviors, cellular pathway activation, and synaptic plasticity. The treatment efficacy and temporal dynamics vary across the different metrics assessed. For example, we observed early effects of the treatment on *Mecp2*$^{-/y}$ behavior, but saw efficacy only at later stages in locomotor activity. This variability could partly be due to the contribution of different brain regions to a given endophenotype and region-specific responses to rhIGF1, given the availability of peripheral IGF1 and the heterogeneous expression pattern of IGF1 receptors in the adult mouse brain (16). The cortex, choroid plexus, and endothelial cells are regions with the highest expression of receptors—the last two are major entry points of systemic IGF1 into the CNS, consistent with the importance of peripheral IGF1 in the maintenance of CNS levels. Nevertheless, the importance of locally synthesized IGF1 in the brain cannot be ruled out, as recent findings show a possible role for environmental enrichment paradigms and active microglia in the production of brain IGF1 (45, 46).

The anxiety measurement we used supports previous findings in mouse models with similar backgrounds and suggests that both sexes of the RTT model have an altered anxiety behavior relative to their WT littermates (1). Some proposed explanations include abnormal perception of safeness or incapability to interpret danger cues in the mutant mice (23). It is worth noting that the results we obtained for anxiety and social measurements from untreated *Mecp2* mutant mice are very similar to those obtained in a PSD95 mutant mouse model, emphasizing the convergence of signaling pathways and synaptic molecules necessary for these behavioral functions (47). Indeed, IGF1 treatment improves excitatory synaptic transmission and motor behaviors in Shank3 haploinsufficient mice (48), and IGF1 application corrects synaptic transmission deficits in iPSC-derived neurons from 22q13 deletion syndrome patients (49), both of which can be attributed to enhanced PSD95 function.

Measuring response amplitude changes and the corresponding shifts in ocular dominance directly tests visual cortical plasticity, and here, for the first time to our knowledge, we describe the effects of a mutated *Mecp2* gene on the course of critical period plasticity. Previous data (5) showed that visual cortical plasticity was present in adult *Mecp2* mutant mice, but whether this was an expansion of the normal critical period or a complete shift in the time window for increased visual cortical plasticity was unknown. Our results support the former explanation, with normal opening of the critical period at P28 as seen by a decreased response from the deprived eye after 4 d of MD, and a persistent state of enhanced plasticity at P60 compared with WT controls, albeit due to enhanced open eye responses. This may represent a form of abnormal synaptic or circuit plasticity following MD (5, 50). IGF1 treatment abolishes this plasticity and stabilizes the underlying circuits and synapses—possibly via effects on inhibitory systems in the cortex (51) or on homeostatic mechanisms (52). The effect on functional circuits in the adult visual cortex reflects the emerging consensus that the consequences of MeCP2 loss are felt throughout life (53–55).

Because serum IGF1 is able to cross the BBB, we attribute the increased activation of brain Akt and ERK to the augmentation of serum IGF1 levels. One correlate of the activation of these pathways is increased synaptogenesis and levels of synaptic PSD95 (27, 56). These results are consistent with previous findings of reduced *PSD95* transcription and protein expression as well as fewer excitatory synapses and spines in *Mecp2* mutant mice (5, 11, 57, 58). The specific mechanisms of IGF1 uptake and clearance in the circulatory system are not completely understood. In normal development, levels of IGF1 peak during puberty (3–4 wk in mice) and decrease in adulthood. Endogenous IGF1 levels are significantly reduced in young *Mecp2*$^{-/y}$ and adult *Mecp2*$^{-/+}$ mice relative to WT mice (Figs. 1*A* and 5*F*). This reduction likely plays a role in the development of RTT neuropathology; treatment beginning from 2 wk of age in *Mecp2*$^{-/y}$ mice increases the total available IGF1 (endogenous plus rhIGF1) and contributes to the improvement of several phenotypes. In older *Mecp2*$^{-/+}$ animals, a short period of rhIGF1 treatment similarly increases total IGF1 availability and improves deficits in breathing patterns, spatial recognition, and anxiety, yet locomotor and social interaction deficits remain unaltered. It is possible that starting treatment earlier, and extending it for longer durations, may lead to greater efficacy in *Mecp2*$^{-/+}$ mice.

Materials and Methods

Detailed information on all items below is provided in *SI Materials and Methods*.

Mice. *Mecp2* hemizygous KO mice and wild-type littermates were obtained by breeding heterozygous females (41) on a C57BL/6J background with male mice on the same background. Adult heterozygous female mice were obtained from Jackson Labs. All experimental protocols were approved by the Animal Care and Use Committee at Massachusetts Institute of Technology and conformed to National Institutes of Health guidelines.

Dosage. Animals were weighed and injected i.p. once every day with either vehicle (saline) or rhIGF1 (Peprotech) dissolved in vehicle. Treatment durations were as noted.

Autonomic Function. Respiratory and cardiac rates were measured in awake mice with a collar sensor pulse oximeter (MouseOx, Starr Life Sciences). Data were filtered and analyzed with Matlab. Breathing patterns were measured using whole-body plethysmography (EMKA Technologies).

Behavioral Assays. For social interaction, mice were tested in a custom-made three-chamber apparatus. Anxiety-related behavior was evaluated in a custom-made plus maze. Ambulatory movement was measured with an automated cage monitor system. Spatial novelty recognition was measured using the open field procedure.

Optical Imaging and Slice Physiology. Methods of animal preparation and data acquisition and analysis for optical imaging were as described previously (5). Cortical sections for slice physiology were prepared as previously described with minor modifications (5).

Histology and Western Blotting. Animals were decapitated and their brain processed for Golgi-Cox stain. For Western blot, the cortex was processed to obtain whole-cell and synaptoneurosome lysates.

Serum Detection. Blood samples were obtained through submandibular puncture. To quantify the levels of mouse and rhIGF1 (R&D Systems), an ELISA test was used.

ACKNOWLEDGMENTS. We thank Alexandra Clemente and Jitendra Sharma, along with members of the M.S. laboratory, for technical assistance. This work was supported by National Science Foundation Graduate Research Fellowship 2388357 (to R.I.G.), a postdoctoral fellowship from the Simons Center for the Social Brain (to S.K. and A.B.), and grants from the National Institutes of Health and the Simons Foundation (to M.S.).

1. Banerjee A, Castro J, Sur M (2012) Rett syndrome: Genes, synapses, circuits, and therapeutics. *Front Psychiatry* 3:34.
2. Chahrour M, Zoghbi HY (2007) The story of Rett syndrome: From clinic to neurobiology. *Neuron* 56(3):422–437.
3. Chahrour M, et al. (2008) MeCP2, a key contributor to neurological disease, activates and represses transcription. *Science* 320(5880):1224–1229.
4. Castro J, Mellios N, Sur M (2013) Mechanisms and therapeutic challenges in autism spectrum disorders: Insights from Rett syndrome. *Curr Opin Neurol* 26(2):154–159.
5. Tropea D, et al. (2009) Partial reversal of Rett Syndrome-like symptoms in MeCP2 mutant mice. *Proc Natl Acad Sci USA* 106(6):2029–2034.
6. Guy J, Gan J, Selfridge J, Cobb S, Bird A (2007) Reversal of neurological defects in a mouse model of Rett syndrome. *Science* 315(5815):1143–1147.
7. Giacometti E, Luikenhuis S, Beard C, Jaenisch R (2007) Partial rescue of MeCP2 deficiency by postnatal activation of MeCP2. *Proc Natl Acad Sci USA* 104(6):1931–1936.
8. Chang Q, Khare G, Dani V, Nelson S, Jaenisch R (2006) The disease progression of Mecp2 mutant mice is affected by the level of BDNF expression. *Neuron* 49(3): 341–348.
9. Zhou Z, et al. (2006) Brain-specific phosphorylation of MeCP2 regulates activity-dependent Bdnf transcription, dendritic growth, and spine maturation. *Neuron* 52(2):255–269.
10. Yoshii A, Constantine-Paton M (2010) Postsynaptic BDNF-TrkB signaling in synapse maturation, plasticity, and disease. *Dev Neurobiol* 70(5):304–322.
11. Ricciardi S, et al. (2011) Reduced AKT/mTOR signaling and protein synthesis dysregulation in a Rett syndrome animal model. *Hum Mol Genet* 20(6):1182–1196.
12. Schmid DA, et al. (2012) A TrkB small molecule partial agonist rescues TrkB phosphorylation deficits and improves respiratory function in a mouse model of Rett syndrome. *J Neurosci* 32(5):1803–1810.
13. Wu D, Pardridge WM (1999) Neuroprotection with noninvasive neurotrophin delivery to the brain. *Proc Natl Acad Sci USA* 96(1):254–259.
14. Nishijima T, et al. (2010) Neuronal activity drives localized blood-brain-barrier transport of serum insulin-like growth factor-I into the CNS. *Neuron* 67(5):834–846.
15. Bondy CA, Cheng CM (2004) Signaling by insulin-like growth factor 1 in brain. *Eur J Pharmacol* 490(1-3):25–31.
16. Fernandez AM, Torres-Alemán I (2012) The many faces of insulin-like peptide signalling in the brain. *Nat Rev Neurosci* 13(4):225–239.
17. Mellios N, et al. (2014) A β-2 adrenergic receptor agonist ameliorates phenotypes and corrects miRNA-mediated IGF1 deficits in an animal model of Rett Syndrome. *Proc Natl Acad Sci USA* 111:9947–9952.
18. Pini G, et al. (2012) IGF1 as a potential treatment for Rett Syndrome: Safety assessment in six Rett patients. *Autism Res Treat* 2012:679801.
19. Khwaja OS, et al. (2014) Safety, pharmacokinetics, and preliminary assessment of efficacy of mecasermin (recombinant human IGF-1) for the treatment of Rett syndrome. *Proc Natl Acad Sci USA* 111(12):4596–4601.
20. Marchetto MCN, et al. (2010) A model for neural development and treatment of Rett syndrome using human induced pluripotent stem cells. *Cell* 143(4):527–539.
21. Li Y, et al. (2013) Global transcriptional and translational repression in human-embryonic-stem-cell-derived Rett syndrome neurons. *Cell Stem Cell* 13(4):446–458.
22. Williams EC, et al. (2014) Mutant astrocytes differentiated from Rett syndrome patients-specific iPSCs have adverse effects on wild-type neurons. *Hum Mol Genet* 23(11):2968–2980.
23. Stearns NA, et al. (2007) Behavioral and anatomical abnormalities in Mecp2 mutant mice: A model for Rett syndrome. *Neuroscience* 146(3):907–921.
24. Gordon JA, Stryker MP (1996) Experience-dependent plasticity of binocular responses in the primary visual cortex of the mouse. *J Neurosci* 16(10):3274–3286.
25. Ehrlich I, Malinow R (2004) Postsynaptic density 95 controls AMPA receptor incorporation during long-term potentiation and experience-driven synaptic plasticity. *J Neurosci* 24(4):916–927.
26. Yoshii A, Sheng MH, Constantine-Paton M (2003) Eye opening induces a rapid dendritic localization of PSD-95 in central visual neurons. *Proc Natl Acad Sci USA* 100(3): 1334–1339.
27. Yoshii A, Constantine-Paton M (2007) BDNF induces transport of PSD-95 to dendrites through PI3K-AKT signaling after NMDA receptor activation. *Nat Neurosci* 10(6): 702–711.
28. Yan H, et al. (2011) Circulating IGF1 regulates hippocampal IGF1 levels and brain gene expression during adolescence. *J Endocrinol* 211(1):27–37.
29. Ishii T, et al. (2001) The role of different X-inactivation pattern on the variable clinical phenotype with Rett syndrome. *Brain Dev* 23(Suppl 1):S161–S164.
30. Amir RE, et al. (2000) Influence of mutation type and X chromosome inactivation on Rett syndrome phenotypes. *Ann Neurol* 47(5):670–679.
31. Xinhua Bao, et al. (2008) X chromosome inactivation in Rett Syndrome and its correlations with MECP2 mutations and phenotype. *J Child Neurol* 23(1):22–25.
32. Samaco RC, et al. (2013) Female Mecp2(+/-) mice display robust behavioral deficits on two different genetic backgrounds providing a framework for pre-clinical studies. *Hum Mol Genet* 22(1):96–109.
33. Katz DM, et al. (2012) Preclinical research in Rett syndrome: Setting the foundation for translational success. *Dis Model Mech* 5(6):733–745, http://dmm.biologists.org/content/5/6/733.long.
34. Weese-Mayer DE, et al. (2006) Autonomic nervous system dysregulation: Breathing and heart rate perturbation during wakefulness in young girls with Rett syndrome. *Pediatr Res* 60(4):443–449.
35. Viemari J-C, et al. (2005) Mecp2 deficiency disrupts norepinephrine and respiratory systems in mice. *J Neurosci* 25(50):11521–11530.
36. Ogier M, et al. (2007) Brain-derived neurotrophic factor expression and respiratory function improve after ampakine treatment in a mouse model of Rett syndrome. *J Neurosci* 27(40):10912–10917.
37. Pitcher MR, et al. (2013) Insulinotropic treatments exacerbate metabolic syndrome in mice lacking MeCP2 function. *Hum Mol Genet* 22(13):2626–2633.
38. Sigmund CD (2000) Viewpoint: Are studies in genetically altered mice out of control? *Arterioscler Thromb Vasc Biol* 20(6):1425–1429.
39. Leiter EH (2002) Mice with targeted gene disruptions or gene insertions for diabetes research: Problems, pitfalls, and potential solutions. *Diabetologia* 45(3):296–308.
40. Berglund ED, et al. (2008) Glucose metabolism in vivo in four commonly used inbred mouse strains. *Diabetes* 57(7):1790–1799.
41. Guy J, Hendrich B, Holmes M, Martin JE, Bird A (2001) A mouse Mecp2-null mutation causes neurological symptoms that mimic Rett syndrome. *Nat Genet* 27(3):322–326.
42. Pratte M, Panayotis N, Ghata A, Villard L, Roux J-C (2011) Progressive motor and respiratory metabolism deficits in post-weaning Mecp2-null male mice. *Behav Brain Res* 216(1):313–320.
43. Ward CS, et al. (2011) MeCP2 is critical within HoxB1-derived tissues of mice for normal lifespan. *J Neurosci* 31(28):10359–10370.
44. Saenger S, et al. (2011) PEGylation enhances the therapeutic potential for insulin-like growth factor I in central nervous system disorders. *Growth Horm IGF Res* 21(5): 292–303.
45. Ciucci F, et al. (2007) Insulin-like growth factor 1 (IGF-1) mediates the effects of enriched environment (EE) on visual cortical development. *PLoS ONE* 2(5):e475.
46. Derecki NC, Cronk JC, Kipnis J (2013) The role of microglia in brain maintenance: Implications for Rett syndrome. *Trends Immunol* 34(3):144–150.
47. Feyder M, et al. (2010) Association of mouse Dlg4 (PSD-95) gene deletion and human DLG4 gene variation with phenotypes relevant to autism spectrum disorders and Williams' syndrome. *Am J Psychiatry* 167(12):1508–1517.
48. Bozdagi O, Tavassoli T, Buxbaum JD (2013) Insulin-like growth factor-1 rescues synaptic and motor deficits in a mouse model of autism and developmental delay. *Mol Autism* 4(1):9–12.
49. Shcheglovitov A, et al. (2013) SHANK3 and IGF1 restore synaptic deficits in neurons from 22q13 deletion syndrome patients. *Nature* 503(7475):267–271.
50. Noutel J, Hong YK, Leu B, Kang E, Chen C (2011) Experience-dependent retinogeniculate synapse remodeling is abnormal in MeCP2-deficient mice. *Neuron* 70(1):35–42.
51. Chao H-T, et al. (2010) Dysfunction in GABA signalling mediates autism-like stereotypies and Rett syndrome phenotypes. *Nature* 468(7321):263–269.
52. Blackman MP, Djukic B, Nelson SB, Turrigiano GG (2012) A critical and cell-autonomous role for MeCP2 in synaptic scaling up. *J Neurosci* 32(39):13529–13536.
53. Nguyen MVC, et al. (2012) MeCP2 is critical for maintaining mature neuronal networks and global brain anatomy during late stages of postnatal brain development and in the mature adult brain. *J Neurosci* 32(29):10021–10034.
54. Cheval H, et al. (2012) Postnatal inactivation reveals enhanced requirement for MeCP2 at distinct age windows. *Hum Mol Genet* 21(17):3806–3814.
55. Guy J, Cheval H, Selfridge J, Bird A (2011) The role of MeCP2 in the brain. *Annu Rev Cell Dev Biol* 27:631–652.
56. Cuesto G, et al. (2011) Phosphoinositide-3-kinase activation controls synaptogenesis and spinogenesis in hippocampal neurons. *J Neurosci* 31(8):2721–2733.
57. Chao H-T, Zoghbi HY, Rosenmund C (2007) MeCP2 controls excitatory synaptic strength by regulating glutamatergic synapse number. *Neuron* 56(1):58–65.
58. Landi S, et al. (2011) The short-time structural plasticity of dendritic spines is altered in a model of Rett syndrome. *Sci Rep* 1:45.

Supporting Information

Castro et al. 10.1073/pnas.1311685111

SI Materials and Methods

Mice. Methyl-CpG binding protein 2 (*Mecp2*) hemizygous-null mice and wild-type (WT) littermates were obtained by breeding heterozygous females (1) supplied by Jackson Lab on a C57BL/6 [B6.129P2(C)-*Mecp2*$^{tm1.1Bird}$/J, Jackson 003890] background with male mice on the same background (Jackson 000664). Heterozygous females ages >6 mo used for testing were obtained directly from Jackson Lab. A total of >150 male and female MeCP2 mice were used for the various assays and measurements. All mice were genotyped as described in the vendor website. Where possible, the genotype of the tested mice was concealed from the investigators while testing was performed. For male mice, the loss of weight and hypoactivity post-4 wk of age presented limitations to complete lack of genotype knowledge. Similarly, older fully symptomatic heterozygous females were strikingly less motile than WT controls.

Dosage and Housing. Homozygous-null mice were grouped with their wild-type siblings and housed at 24 °C and variable humidity in a 12 h light cycle (7:00 AM to 7:00 PM). Animals were weighed and injected i.p. once daily starting on postnatal day 14 (P14) with either vehicle (saline) or 0.25 mg/kg full-length (70 aa) recombinant human insulin-like growth factor-1 (IGF1) (Peprotech) dissolved in saline with 0.01% BSA (wt/vol). Due to safety concerns, namely the risk of internal organ damage and the volume of injection that could prove fatal, we considered P14 the earliest age to begin safely injecting the animals. Wild-type male mice were euthanized at 15 wk of age. Hemizygous-null mice were terminated when they lost more than 20% of their body weight in 1 wk. Heterozygous females were kept in individual home cages and injected with a 10× dose of recombinant human IGF1 (rhIGF1) daily for 3 wk.

Behavioral Analyses: Social Assay. Mice were tested in a custom-made social approach apparatus (2) consisting of an acrylic box with a white floor for high contrast and three subdivisions. Each side compartment contained a clear perforated acrylic cylinder that allowed sniffing and visual interaction between the tested and stimulus mouse. Animals were tested at 5 and 8 wk of age with unrelated, age- and background-matched wild-type stimulus mice. Behavior testing was done during the light cycle at least 2 h after injection. The animals were acclimatized by exposing them to the apparatus for 5 min for 2 consecutive days before the test. The test animal was first placed in the middle chamber and allowed to freely move for 5 min while being video recorded. The test mouse was then removed and a stimulus mouse was placed in the cylinder of one of the side chambers for 5 min for acclimatization. The test mouse was immediately reintroduced into the middle chamber and its behavior recorded for 10 min. The cage was cleaned thoroughly with Quatricide PV (Pharmacal) after each experiment, and a second 5-min test was recorded after 30 min with the same stimulus mouse. Different stimulus mice were used each week.

Video recordings were analyzed with custom-made ImageJ macros that measured the total amount of time spent in each chamber and the number of times that the test animal crossed from one chamber to the other. Only animals with more than eight crosses were included in the analysis.

Behavioral Analyses: Anxiety Assay. Anxiety-related behavior was evaluated on a plus maze. The maze was made of a solid color smooth acrylic plastic and consisted of a center square (5 cm × 5cm) and four arms: two open without walls and two closed with a 15-cm-high wall. Each arm of the maze measured 30 cm long and 5 cm wide and was supported by a 40-cm-high leg. Four-week-old animals were placed in the center square always facing the same open arm and were allowed to explore the maze freely for 5 min while being videotaped. Mice were not preexposed to the setup to avoid test-decay effects due to increased acclimatization to the environment. After the test, the mice were removed from the maze and all of the surfaces cleaned with Quatricide before testing the next animal. The amount of time spent in each arm and the number of crossings into the center square were analyzed by custom-made ImageJ macros.

Behavioral Analysis: Spatial Novelty Recognition. The behavioral analysis of spatial novelty recognition was modified from an open field assay previously described (3). For the spatial novelty recognition test, mice were placed in an arena for six sessions, each lasting 6 min. Between each session mice were transferred to their home cages for 3 min and the arena cleaned. During the first session, mice explored the empty area, after which four objects of similar size yet different shapes were added inside. Object exploration was monitored and data collected using video recording above the arena. The mice were allowed to explore the objects during sessions 2–5, and the average contact duration with each object was assessed. On the sixth session, two objects were spatially rearranged. A performance ratio was calculated as the ratio of the time spent in contact with the displaced objects (DOs) versus the non-DOs (NDOs) during the last trial divided by the ratio of the time spent in contact with the DOs versus the NDOs during the fourth trial.

Breath Rate and Cardiac Monitoring. Each mouse was tested once a week for 2 wk, and the data were pooled by age for weeks 4–5 or 7–8. Heart and breath rates were monitored using a pulse oximeter collar sensor (MouseOx, Starr Life Sciences). One day before testing, mice were depilated around the neck for improved sensor readings, and blank collar clips were used to acclimatize the animal to the oximeter collar clip before each test. Mice were awake and restrained in a tube for 10-min sessions. Heart rate (beats per minute) and breath rate (breaths per minute) were recorded continuously for each animal by the device and pooled for group-wide comparisons.

Plethysmography Recordings of Breathing Patterns. Breathing patterns were recorded in unrestrained and unanesthetized mice using a whole-body flow plethysmograph (EMKA Technologies) in which a constant bias flow supply connected to the animal recording chamber ensured continuous inflow of fresh air (0.8 L/min). Mice were habituated in the plethysmograph chamber to reduce any stress before measurements. For each female mouse, the inspiratory time (T_i), expiratory time (T_e), peak expiratory flow (PEF), and breath holds (defined as T_e times lasting longer than 500 ms) were measured during 12-min periods, once before treatment began and then again after 3 wk of treatment.

Locomotion Assay: Ambulatory Movement. Spontaneous locomotor activity was measured with the use of an infrared beam device monitoring movement in a cage (PhenoMaster-Activity XY, TSE Systems, Inc.). For each experiment, a mouse was acclimatized to the cage for at least 1 h before recordings started. Movement was measured every minute for 11 h during the 12 h dark cycle (7:00 PM to 7:00 AM). The number of beam crossings per minute for each animal was pooled for group-wide comparisons.

Western Blotting. Synaptoneurosomes were prepared as described previously (4). *Mecp2*-null mice and wild-type controls were decapitated, and the brain tissue extracted and immediately dissected on ice-cold PBS. For each brain, half the cortex and cerebellum was homogenized in ice-cold homogenization buffer [10 mM Hepes, 2 mM EGTA, 2 mM EDTA, 1% SDS, 1× phosphatase inhibitor mixture (Roche), protease inhibitor mixture (Roche)], while the other half was homogenized in synaptoneurosome buffer [10 mM Hepes, 2.0 mM EDTA, 2.0 mM EGTA, 150 mM NaCl, phosphatase inhibitor mixture (Roche), protease inhibitor mixture (Roche)], with 20 even strokes in a glass–glass homogenizer. The synaptoneurosome homogenate was first passed through two 105 μm nylon mesh (Sefar America) filters and then through a 5 μm nitrocellulose filter (Millipore), and finally centrifuged at 1,000 × *g* for 10 min at 4 °C. The synaptoneurosome pellet was resuspended in buffer. Aliquots of all of the homogenized tissue were stored in –20 °C until SDS/PAGE analysis. BCA protein assay kit (BioRad) was used to determine the protein concentration of each homogenate and synaptoneurosome sample.

Whole-cell (10 μg) or synaptoneurosome (5 μg) samples were loaded on 4–15% polyacrylamide gels (BioRad), transferred to PVDF membranes (Millipore), and immunoblotted for protein expression using the following antibodies: total Akt (1:1,000, Cell Signaling), phospho (Ser473) Akt (1:500, Cell Signaling), PSD-95 (1:1,000, Cell Signaling), total ERK1/2 (1:1,000, Cell Signaling), phospho (Thr202/Tyr204) ERK1/2 (1:2,000, Cell Signaling), GAPDH (1:4,000, Abcam), and Tubulin (1:250,000, Sigma-Aldrich). Blots were then incubated with appropriate secondary antibodies coupled to HRP (1:4,000, Cell Signaling). Immunoreactive bands were detected by enhanced chemiluminescence (Supersignal West, PicoCL or FemtoCL, Fisher Scientific). Optical densities of detected bands were quantified using ImageJ software. A standard sample of wild-type mouse cortical tissue was run on each gel to gauge blot-to-blot variability.

Golgi Stain. To measure spine density, P42 male mice were used. Animals were decapitated and brains were dissected out and processed using a Golgi-Cox stain kit (FD Rapid Golgistain, FD Neurotechnologies), following kit protocol. Images were taken in a Zeiss Axioscope with a 63× high numerical aperture (1.4) oil immersion objective. Analysis was done with ImageJ.

Measurement of Recombinant Human and Endogenous IGF1 Levels. To quantify levels of recombinant human and mouse IGF1 in blood serum, a solid-phase ELISA test (Quantikine ELISA, R&D Systems Inc.) was used as per kit instructions. Blood samples were obtained through submandibular puncture and collected in serum-separating tubes with clot activator (Sarstedt AG & Co.). The tubes were left to sit for 30 min, centrifuged at 10,000 × *g* for 5 min, and the collected serum frozen. For analysis, serum was pretreated to release IGF1 from binding protein and incubated for 2 h to attach the IGF1 to the plate. A human IGF1 conjugate was added for 1 or 2 h depending on the IGF1 type. Finally, a substrate solution was incubated for 30 min to elicit a colorimetric reaction that was stopped with sulfuric acid. The optical density was measured within 10 min of the end of the assay using a microplate reader (iMark, Bio-Rad) set at 450 nm and with a wavelength correction of 550 nm.

Optical Imaging of Intrinsic Signals. Optical imaging of intrinsic signals was used to evaluate the relative strength of responses elicited by the deprived and undeprived eye during the presentation of visual stimuli (5). Imaging experiments were carried out in P28 males and females as well as adult (>P60) female mice as described previously (6). For monocular deprivation, mice were anesthetized with avertin (0.016 mL/g), and the eye contralateral to the imaged hemisphere was sutured for 4 d before the imaging session.

For imaging, mice were anesthetized using urethane (1.5 g/kg) and chloroprothixiene (1%). The head was fixed in a stereotaxic frame and the skull exposed and cleaned. The skull was thinned over primary visual cortex (V1) using a dremel drill. The cortical surface was illuminated with a tungsten halogen light source, and a slow-scan video camera equipped with a tandem macrolens arrangement was used to acquire images of intrinsic signals. First, the cortical surface was illuminated with a green filter (550 nm) to obtain a reference image of the surface blood vessels. Next, the focal plane was adjusted to about 300 microns below the cortical surface, and a red filter (630 nm) was used for the acquisition of intrinsic signals. To measure the relative cortical activation, a drifting bar (four orientations, spatial frequency of 9 degrees per cycle) was presented to each eye individually. Eye patches were used to deliver the stimulation to each eye separately. Image analysis was performed with custom-made software (MATLAB). The Ocular Dominance Index (ODI) was defined as the difference between contralateral and ipsilateral eye responses divided by their sum and used to evaluate the relative strength of eye-evoked cortical activation.

Slice Electrophysiology. Control and *Mecp2* mutant mice (P27–29) were anesthetized by isofluorane inhalation. The brains were rapidly removed after decapitation and submerged into 4 °C slicing buffer containing the following (in mM): 130 NaCl, 10 glucose, 1.25 NaH_2PO_4, 24 $NaCHO_3$, 3.5 KCl, 6 $MgCl_2$, and 0.5 $CaCl_2$. They were then bubbled with 95% O_2 and 5% CO_2. Brains were sliced coronally at a thickness of 300 μm on a vibratory microtome VT1200 (Leica). After slicing, sections were incubated for 20 min in room temperature artificial cerebral spinal fluid (ACSF) and bubbled continuously with 95% O_2 and 5% CO_2. The ACSF contained the following (in mM): 130 NaCl, 10 glucose, 1.25 NaH_2PO_4, 24 $NaCHO_3$, 3.5 KCl, 2.5 $CaCl_4$, and 1.5 $MgCl_2$.

For recording of AMPA receptor miniature excitatory postsynaptic currents (mEPSCs), whole-cell patch clamp of V1 layer 2/3 pyramidal neurons was performed using pipettes (5.0–6.0 Mohm resistance) filled with an internal solution containing (in mM): 120 $CsMeSO_4$, 10 TEA-Cl, 5 EGTA, 10 NaCl, 5 Mg-ATP, 0.4 Na-GTP, and 10 Hepes, pH 7.2–7.3, with 1 M CsOH. Neurons were identified by their location and morphology and voltage clamped at a membrane potential of −70 mV. Neurons were recorded at room temperature (25 °C) in ACSF containing 1 μM TTX and 50 μM picrotoxin. AMPA receptor mEPSCs were blocked with application of 10 μM 6-cyano-7-nitroquinoxaline-2,3-dione (CNQX).

Membrane currents were recorded using a Multiclamp 700B (Axon Instruments) at 10 kHz and filtered at 2 kHz. Traces were analyzed for EPSCs in Clampfit 10.2 software (Axon Instruments) using a template constructed from four to six mEPSCs intrinsic to each recording. Cumulative probability was calculated for interevent interval and peak amplitude and subjected to the Kolmogorov–Smirnov test for significance.

Data Analysis. Analysis for male and female mice were performed separately using Student *t* test, paired *t* test (females), and one-way ANOVA with either Newman–Keuls or Tukey's post hoc analysis for multiple comparisons. ODI comparisons were analyzed with Mann–Whitney rank sum test for nonparametric data. Analysis was performed using either MATLAB or Prism.

1. Guy J, Hendrich B, Holmes M, Martin JE, Bird A (2001) A mouse Mecp2-null mutation causes neurological symptoms that mimic Rett syndrome. *Nat Genet* 27(3):322–326.

2. Page DT, Kuti OJ, Sur M (2009) Computerized assessment of social approach behavior in mouse. *Front Behav Neurosci* 3:48.

3. Stearns NA, et al. (2007) Behavioral and anatomical abnormalities in Mecp2 mutant mice: A model for Rett syndrome. *Neuroscience* 146(3):907–921.
4. Wells DG, et al. (2001) A role for the cytoplasmic polyadenylation element in NMDA receptor-regulated mRNA translation in neurons. *J Neurosci* 21(24):9541–9548.
5. Tropea D, Majewska AK, Garcia R, Sur M (2010) Structural dynamics of synapses in vivo correlate with functional changes during experience-dependent plasticity in visual cortex. *J Neurosci* 30(33):11086–11095.
6. Tropea D, et al. (2009) Partial reversal of Rett Syndrome-like symptoms in MeCP2 mutant mice. *Proc Natl Acad Sci USA* 106(6):2029–2034.

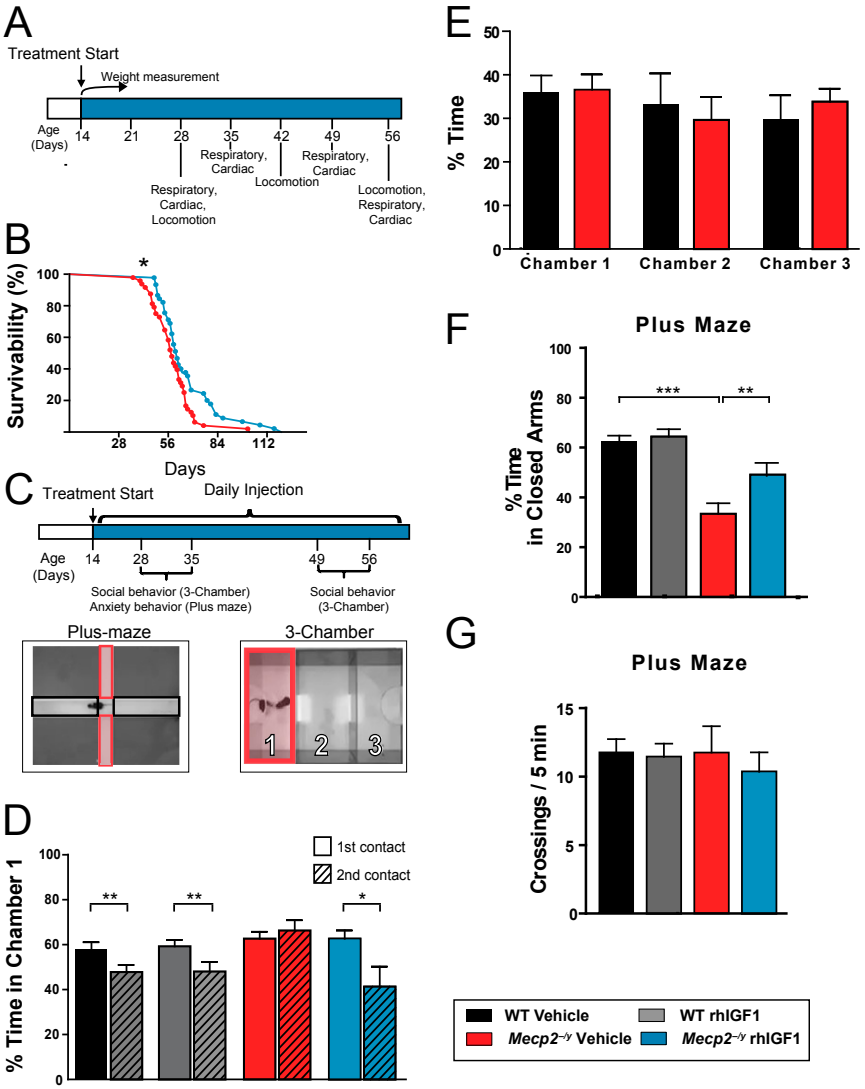

Fig. S1. (*A*) Timeline for experimental schedule of physiological measurements. (*B*) Kaplan–Meier survival plot of *Mecp2* mutant animals treated with vehicle or rhIGF1 (Mantel–Cox test). (*C*) Experimental timeline for behavioral tests (*Upper*). Overhead views of the custom-made elevated plus maze apparatus used to measure anxiety with open and closed arms, respectively, outlined in red and black (*Lower Left*) and three-chamber apparatus used to test social behavior with first chamber highlighted in red (*Lower Right*). (*D*) Three-chamber test measurements showing the percentage of time the animals spent socializing with a stranger mouse during the first contact (solid bars) and 30 min after the first contact (hatched bars) at P56 (paired *t* test). (*E*) Percentage of time spent in each chamber in an empty three-chamber apparatus. Animals do not show any chamber preference when exposed to an empty arena (one-way ANOVA test). (*F*) Percentage of time spent in the closed arms of the plus maze (ANOVA with Newman–Keuls post hoc analysis). (*G*) Basal locomotor activity of the animals during the plus maze test measured by the number of entries into open arms per session. Please refer to Fig. 1 for number of animals per group in each experiment. Error bars represent SEM. $*P < 0.05$; $**P < 0.01$; $***P < 0.001$.

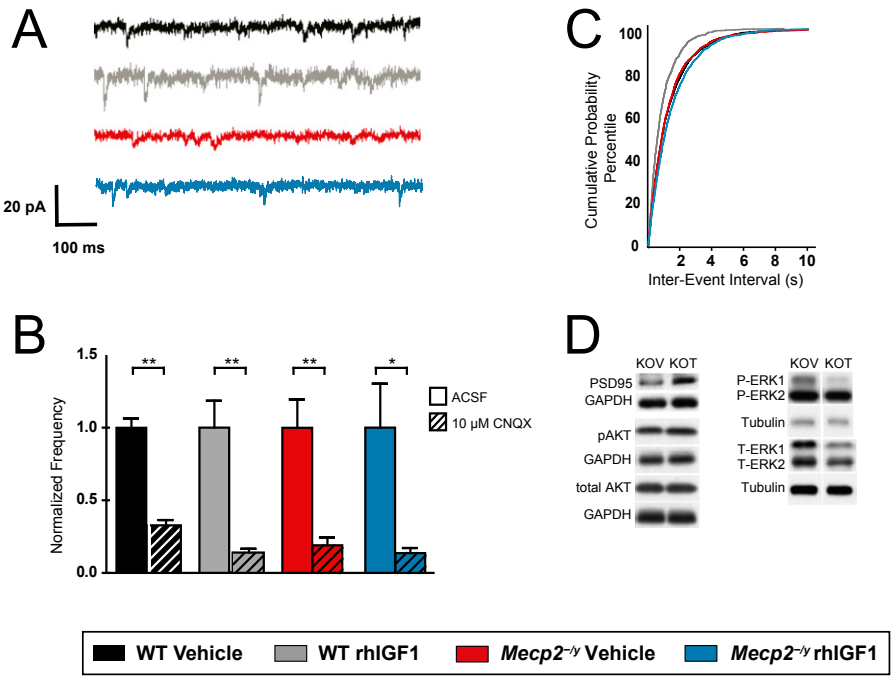

Fig. S2. (*A*) Representative trace of mEPSCs recorded from V1 layer 2/3 pyramidal neurons for all groups. (*B*) Normalized frequencies of mEPSCs recorded from layer 2/3 pyramidal neurons. Populations were normalized to their respective ACSF frequency average value. Incubation with 10 μM of CNQX drastically reduced the activity, indicating that the mEPSCs depend largely on AMPA receptors (paired *t* test). (*C*) Population distribution of the interevent interval. (*D*) Representative Western blot images of proteins measured. Please refer to Fig. 3 for number of animals per group in each experiment. Error bars represent SEM. $*P < 0.05$; $**P < 0.01$.

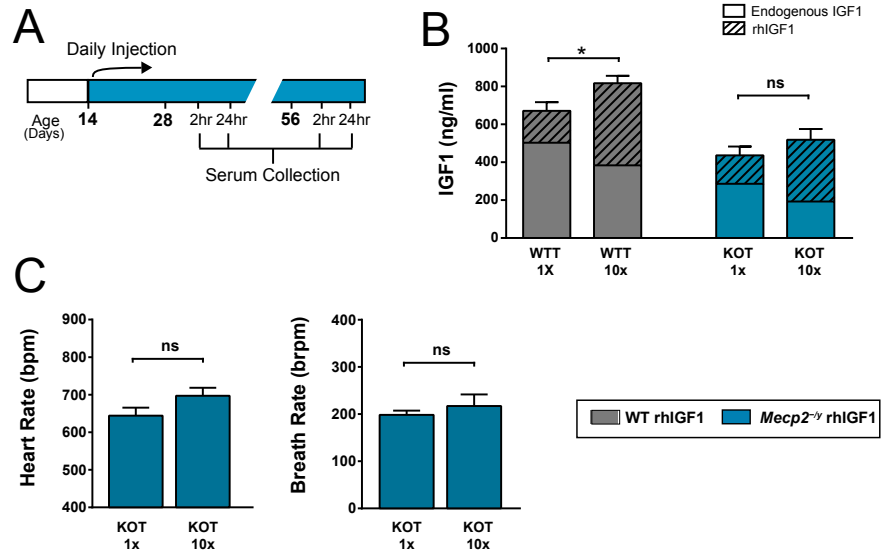

Fig. S3. (*A*) Timeline for serum collection. (*B*) Total IGF1 concentration in blood serum collected 2 h postinjection when animals were treated with a normal dose (0.25 mg/kg, 1×) or at 10 times the concentration (2.5 mg/kg, 10×), calculated by addition of endogenous (filled boxes) and rhIGF1 levels (hatched boxes) for each animal. Statistics were calculated with the summed values (unpaired *t* test; WT 1×, $n = 10$; 10×, $n = 7$; *Mecp2*$^{-/y}$ 1×, $n = 11$; 10×, $n = 5$). (*C*) Average cardiac (*Left*) and breathing (*Right*) rates of *Mecp2* KO animals treated with the regular or 10× dose (unpaired *t* test; *Mecp2*$^{-/y}$ 1×, $n = 14$; 10×, $n = 5$ for each). Error bars represent SEM. $*P < 0.05$; ns, not significant.

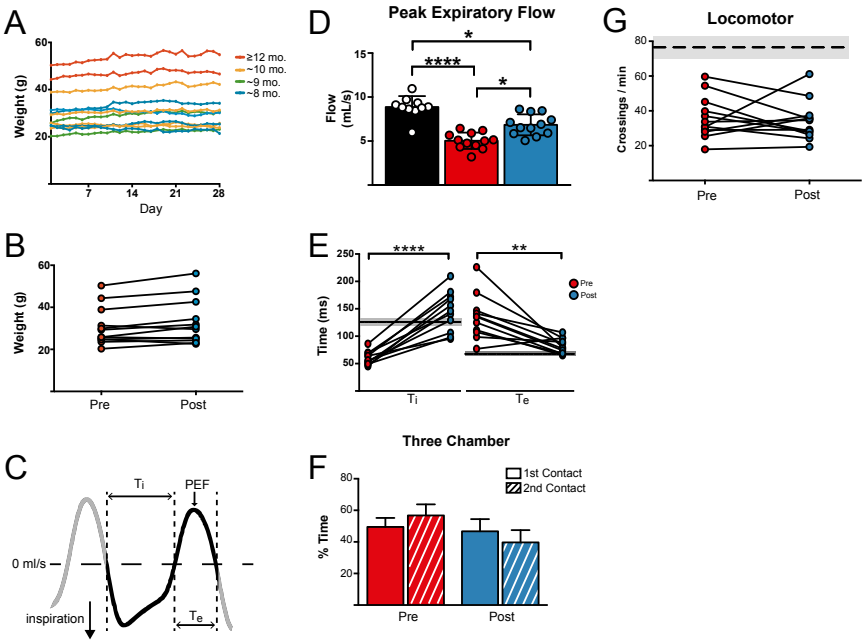

Fig. S4. (*A*) Weights of individual animals measured daily from the beginning of treatment until 4 wk later, 1 wk after treatment ended. Color coded by age of each individual female (see key). (*B*) Comparison of weight of each animal at the beginning and end of treatment period shows no decrease or statistical difference (paired *t* test). (*C*) Diagram representing calculation for inspiratory time (T_i), expiratory time (T_e), and peak expiratory flow (PEF) of a sample breath. (*D*) Scatter plots and means of PEF amplitude of female mice in each group showing a significant reduction in *Mecp2*$^{-/+}$ mice before treatment and a significant increase posttreatment (ordinary one-way ANOVA with Tukey's post hoc analysis for multiple comparisons; dots represent individual animals). (*E*) Individual paired measurements of total T_i and T_e (paired *t* test). Dashed line and shaded area indicate WT mean and SEM, respectively. (*F*) No significant shift in percentage time spent in chamber with stranger mouse between first and second exposure pre- and posttreatment. (*G*) No difference in the average number of beam crossings during paired measurements of nocturnal locomotor activity (paired *t* test). *Mecp2*$^{-/+}$ mice were considerably more hypoactive than females in the WT control group. Dashed line and shaded area indicate WT mean and SEM, respectively.